Vehicle-to-Vehicle Millimeter-Wave Channel Measurements at 56-64 GHz

Jiri Blumenstein*, Ales Prokes*, Josef Vychodil*, Tomas Mikulasek*,
Erich Zöchmann†‡, Herbert Groll‡, Christoph F. Mecklenbräuker‡,
Markus Hofer^x, Thomas Zemen^x, Seun Sangodoyin††, Andreas Molisch††

* *Department of Radio Electronics, Brno University of Technology, Czech Republic,* blumenstein@vutbr.cz
† *Christian Doppler Laboratory for Dependable Wireless Connectivity for the Society in Motion*
‡ *Institute of Telecommunications, TU Wien, Austria*
^x *Safety and Security Department, Austrian Institute of Technology, Austria*
†† *Wireless Devices and Systems Group, University of Southern California, USA*

***Abstract*—This paper presents results obtained from a vehicle-to-vehicle channel measurement campaign carried out in the millimeter-wave band around a 60 GHz center frequency and with 8 GHz of bandwidth. We characterize a situation of two oncoming cars on a two-lane road in the campus of the Brno University of Technology. For several vehicle passes we evaluate: (1) observed root mean square (RMS) delay spreads as a function of the received power, (2) temporal decorrelation of the channel impulse response and (3) a dependency of the Pearson correlation coefficient on the received power. For the measurement campaign, a correlative time-domain channel sounder was used.**

***Index Terms*—mm-wave, channel measurement, vehicle-to-vehicle, channel delay spread**

I. Introduction

The millimeter wave (mmwave) band has been in the focus of the research community for decades, see, e.g., [1]. However, thanks to the inclusion of this band in the 5G standard [2] and thanks to the fact that mmwave bands offer several GHz of unlicensed bandwidth for industrial scientific and medical (ISM) purposes, the interest has greatly increased over the past few years. Literature on the general mmwave channel characterization has made considerable progress, see, e.g., an overview in [3]. In [4], a vehicle-to-vehicle (V2V) scenario is discussed and path-loss and fading characteristics are derived; however, with a rather limited bandwidth of 400 MHz at 73 GHz center frequency. A narrow-band car-to-car communication with a 1 Mb/s data transmission in the 60 GHz band was investigated in [5] already in 2001. For vehicular mm-wave channels, the number of investigations is more limited. Refs. [6]–[9] deal with specific phenomena like vibrations and road surface quality influence on a Doppler spread. Clearly, aiming at multi-GB/s data transmissions required for the future V2V and vehicle-to-infrastructure (V2I) links [10], several GHz of bandwidth are needed. Therefore, the wide-band channel characterization of the V2I environment is studied in [11]. An example of a V2V measurement campaign is published in [12]. Here, the transmitter (TX) and receiver (RX) are stationary, while the surrounding traffic causes a time-variant nature of the channel. It is worth noting that few vehicle-to-vehicle measurements of the wide-band channel have been published due to obvious complications with a precise synchronization of the mutually moving TX and RX which can not be done simply via a classical 10 MHz coaxial cable. In this paper we overcome this issue by means of stable local oscillators. Our measurement is done for a frequency band spanning 56 GHz to 64 GHz utilizing a correlative time-domain channel sounder presented, e.g., in [13]. Specifically, this paper contributes to the mmwave V2V wide-band channel characterization as follows:

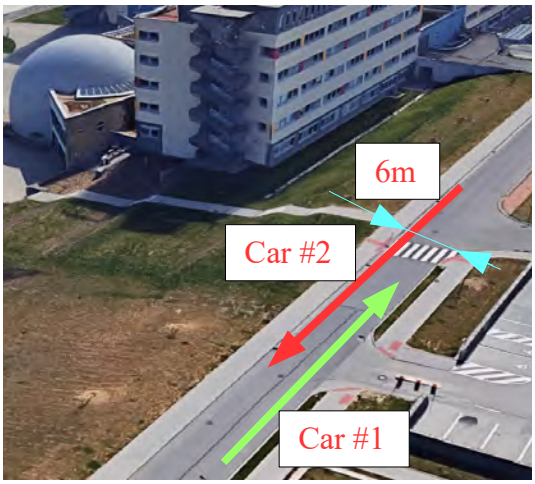

Fig. 1. The test site. Two cars driving in opposite direction on a two-lane road. Several passes ware performed at speeds within the city speed limit (50 km/h).

- We present exemplary results of V2V channel measurement campaign performed for two oncoming cars during subsequent events: (1) driving towards each other, (2) passing and (3) driving away from each other.
- We evaluate the RMS delay spread for a number of vehicle passes as a function of received power.
- Moreover, we investigate the temporal decorrelation of the channel, more precisely, we show how the Pearson correlation coefficient of the channel impulse responses (CIRs) decreases with time difference of the reception.

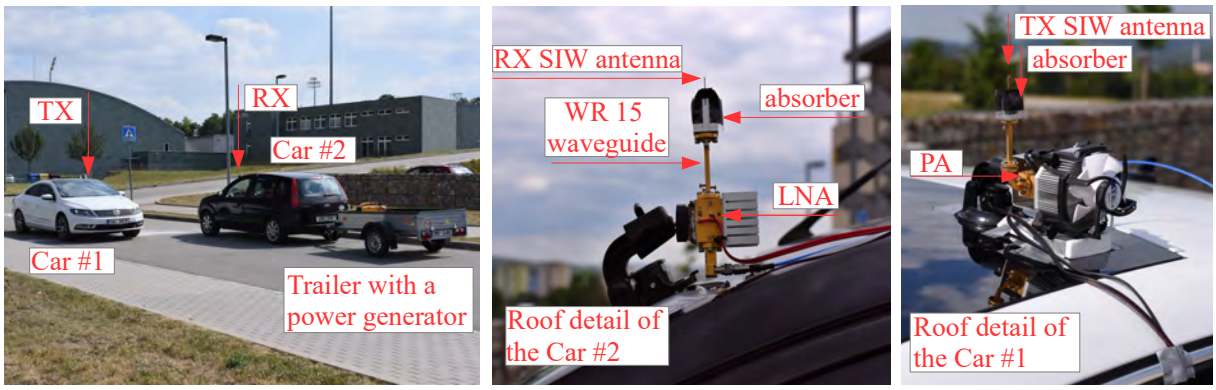

Fig. 2. Photographs taken during the measurement campaign. Two measurement vehicles, Car #1 (with a battery pack in the trunk) and Car #2 (with a 2 kW gas-powered generator on the depicted trailer) at their approximate meeting point. Picture of TX and RX mounting including PA and LNA installation detail.

II. Description of the Measurement Scenario

A. Test-Site Characterization

The measurement campaign was performed on the campus of the Brno University of Technology, in the city of Brno, Czech Republic. The location and controlled traffic ensures a non-obstructed line-of-sight (LOS) during the whole CIR recording time. In fact, no other participating cars nor notable moving objects were present during the measurements. There are no buildings around the immediate perimeter of the driven two-lane road; however, there is a university building around 50 m from the notional meeting point of the passing vehicles. In Figure 1, we depict the location from the bird-eye's view.

B. Measurement Vehicles and RX and TX hardware

We utilize two vehicles labeled as car #1 and #2, where #1 carries the TX and #2 the RX, as seen in Figure 2. In order to provide the TX and RX hardware with electricity, the TX was powered by a large battery pack loaded in the trunk, while the RX was supplied by a gas-powered generator loaded on the trailer, as depicted in Figure 2.

As for the utilized antennas, omni-directional substrate integrated waveguide (SIW) antennas presented in [14], [15] were used both at the RX and TX sides. The mounting of the antennas was done by suctions caps on the top-left corners (from the driver's perspective) of the measurement vehicle's windshields.

III. Channel Sounder

The time-variant radio propagation channel is defined by the CIR and, written as [16]:

$$h(t,\tau) = \sum_{n=1}^{N(t)} \alpha_n(t) e^{j2\pi\nu_D t} \delta\left(\tau - \tau_n(t)\right), \qquad (1)$$

where N is the number of propagation path components characterizing the amount of channel reverberation. Note that in this measurement campaign, the LOS components are always present. The variables $\alpha_n(t)$ and $\tau_n(t)$ corresponds to the amplitude and delay of the n-th propagation path while δ is the Dirac impulse and ν_D is the Doppler frequency. Exploiting Golay sequences [17] with a triangular autocorrelation function R_{xx} as a sounding (transmitted) signal $x(t)$, the received signal $y(t)$ is given as (neglecting noise here for convenience of notation):

$$y(t) = h(t) \otimes x(t), \qquad (2)$$

where $\otimes$ stands for the linear convolution. The CIR estimate is then determined from the cross-correlation of the received and transmitted signals $x(t)$ and $y(t)$ is written as:

$$R_{xy}(\tau) = \mathrm{E}\{x^*(t)y(t)\} = h(t) \otimes R_{xx}(t) \approx$$
$$\approx h(t) \otimes \delta(\tau) = h(t), \qquad (3)$$

where $\mathrm{E}\{\}$ denotes for the expected value operator. More details on this method is available in [18].

A. Calibration and Synchronization

The utilized correlative time-domain channel sounder is based on our previous work, e.g. described in [13], [19]. The main difference here is that the TX and RX parts are galvanically separated in order to allow the mutual movement, as required by the V2V scenario. The synchronization is achieved via a calibration process which requires back-to-back connection of the WR15 TX waveguide output with the input of the RX through a continuously adjustable attenuator in order to calibrate the system for a correct transmit power avoiding RX overdrive. The TX power is then kept constant for the whole measurement. After the calibration and fastening of the SIW antennas (which are not part of the calibration), the synchronization is held by rubidium (Rb) oscillators, whose specifications are given in [20]. The block diagram of the utilized time-domain channel sounder is shown in Figure 3.

B. Components and Parameters

The time-domain channel sounder is built from standard laboratory devices and off-the-shelf parts. We utilize a Tektronix MSO72004C Mixed Signal Oscilloscope performing a matched reception with 50 GS/s sampling frequency and 20 GHz bandwidth. This received signal is filtered in the base-band with a microstrip low-pass filter with 8 GHz bandwidth.

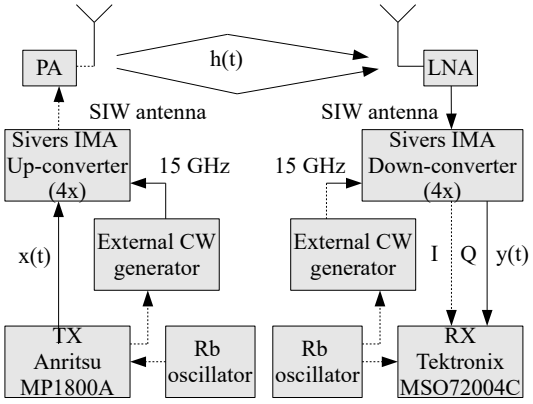

Fig. 3. Time-domain correlative channel sounder utilizing Golay sequences, omni-directional SIW antennas and local rubidium oscillators.

In order to tackle the nonlinearities of the measurement setup, in particular the nonlinearities of the power amplifier (PA), we employ distinct repetition pattern of the transmitted complementary Golay sequences. We transmit two complementary sequences, each 4-times repeated with different polarity. This method is elaborated in [13], [19]. The repetition of the transmitted signal in the time domain also increases the correlation gain, which is needed in order to overcome the path-loss at 60 GHz with 8 GHz of bandwidth. The basic length of the sequence is $\mathrm{L} = 2048$ and the correlation gain is given as $10\log(4\mathrm{L}) = 39.1$ dB. Then, the signal is up-sampled leading to a length of the sequence being $4 \times 8\mathrm{L} = 65536$ samples. With the 50 GS/s sampling frequency we are able to store 492 channel snapshots into the fast internal memory of the oscilloscope (31.25 MS). We set an artificial time lag of $\mathrm{T_L} = 9.93$ ms in between subsequent pseudorandom binary sequence (PRBS) transmissions in order to obtain a total channel recording time $\mathrm{T} \approx 4.6$ s.

The TX part consists of an Anritsu Signal Quality Analyzer MP1800A which generates a wide-band PRBS (in our case the mentioned Golay sequences) with 12.5 Gbit/s data rate and 13 dBm output power. The dynamic range is extended via the low-noise and power amplifiers QuinStar QLW-50754530-I2 (gain of 35 $\pm$3 dB) and QPW-50662330 (with a gain of 33 $\pm$3 dB and a noise figure of 4.5 dB) respectively. In order to move the signal to the desired mmwave band, we utilize the Sivers IMA FC1003V/01 up-/down-converter. The attenuation of coaxial cables used for connecting either the PA or LNA with the up-/down-converters is 12 dB.

IV. Measurement Results

As an exemplary data set of the measured CIRs for one pass of the measurement vehicles, we depict Figure 4. The CIRs exhibit typical properties that could be related to the mentioned driving situations. Via a visual inspection we distinguish:

1) the vehicles #1 and #2 are directly approaching each other in the time interval $t \in [0, 2.4)$ s and the received power increases with a delay dispersion of the channel.
2) The cars meet each other at time $t \approx 2.4$ s with a minimal mutual distance of approx. 3 m, while the received energy and the delay dispersion are maximized.
3) The measurement vehicles are driving away from each other in the time interval $t \in (2.4, 4.6]$ s. The received power decreases with time and exhibits variations, probably due to a slight ripple of the rear half-sphere of the radiation pattern of the antennas, as visible in [14].

As mentioned in previous section, the CIR recoding covers approximately 4.6 s. The depicted data are normalized (i.e. $\max(|h(t,\tau)|) \triangleq 1$) and thresholded such that all components with the amplitude below 0.1 are neglected.

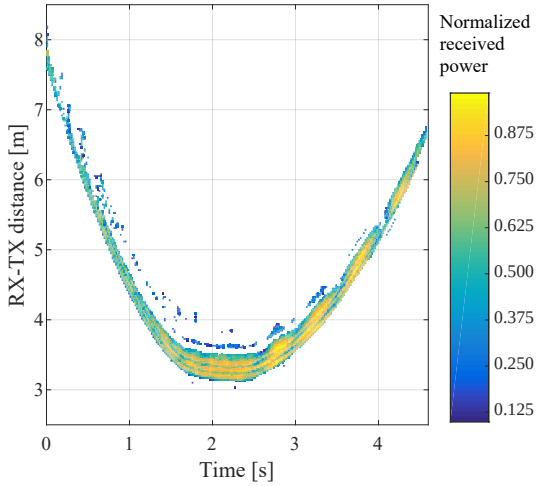

Fig. 4. Exemplary channel impulse recording of one pass of the vehicles. The measured data are thresholded, therefore the noise background is not depicted.

A. The channel delay dispersion

In the literature (see e.g. [21]), the delay dispersion of the channel is often evaluated via the root mean square (RMS) delay spread and is defined as:

$$\sigma_{\mathrm{RMS}}(t) = \sqrt{\frac{\int_0^\infty (\tau - \bar{\tau}^2) P(t,\tau)}{\int_0^\infty P(t,\tau)}}, \text{ where } \bar{\tau} = \frac{\int_0^\infty \tau P(t,\tau)}{\int_0^\infty P(t,\tau)} \tag{4}$$

where τ is the time delay, i.e. the y-axis in Figure 4 and

$$P(t,\tau) = \lim_{t \to T_s} \frac{1}{2T} \int_0^{T_s} |h(t,\tau)|^2 dt, \tag{5}$$

where T_s is the time region where quasi-stationarity is valid [21]. It is evident, that typical dimensions of the quasi-stationarity regions are highly dependent on the geometry and other relevant properties of the V2V scenarios (see e.g. [11]). This measurement campaign has eliminated surrounding traffic; consequently the LOS component and possible reflections from the measurement cars are the dominant sources of the received signal. In this case, the practically achieved results of the RMS delay spread are evaluated for each measured CIR for several passes of the vehicles in Figure 5. Please note that individual CIRs are aligned by the LOS (maximal) component.

Here, we define 8 power bins such that the summed received power $\sum_\tau P(t,\tau)$ for each individual measurement falls into one bin of a uniformly divided interval $[0.3, 1]$. In Figure 5, each gray point represents one measured CIR and it is noticeable that the higher the received power, the higher the RMS delay spread. The intuition behind this result is, that the reflections with lowest received power are simply buried under the noise floor and do not contribute to the RMS delay spread. Due to the mobile nature of the channel, it is not possible to average out the noise in (5), as one could do in a stationary environment. In order to illustrate the phenomena of the rising RMS delay spread with the received power, the mean values of the observed RMS delay spread are evaluated for each power bin and are shown as a blue cross. The variances of the corresponding dataset are depicted as the error bars. The mean values are linearly regressed to highlight the trend.

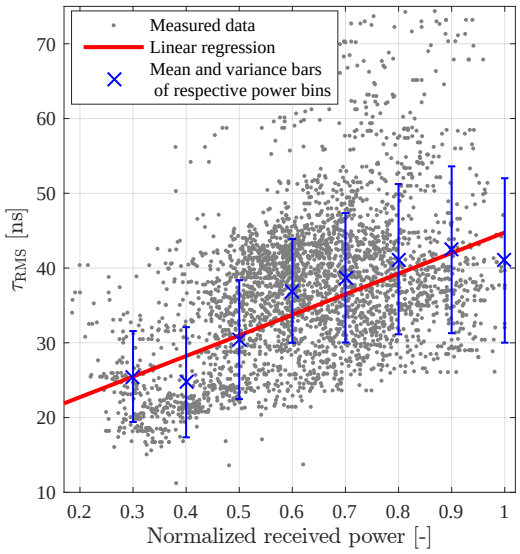

Fig. 5. Measured RMS delay spread for passing cars including mean and variance evaluation for respective normalized received power bins. Mean values of the respective power bins are linearly regressed.

B. The Channel Correlations

The channel quasi-stationarity time T_s, as discussed in the previous section, is a time duration over which the channel statistics do not change noticeably [21]. In order to evaluate the level of change, we employ the Pearson correlation coefficient (as in [22]), which is given as:

$$\rho(\Delta t) = \frac{\mathrm{E}[h'(t) - \mu_{h'(t)})(h'(t+\Delta t) - \mu_{h'(t+\Delta t)})]}{\sigma_{h'(t)}\sigma_{h'(t+\Delta t)}}, \quad (6)$$

where $h'(t) = |h(t,\tau)|^2$ and $\sigma_{h'(t)}$ denotes the standard deviation while $\mu_{h'(t)}$ is the mean value of $h'(t)$. The correlations are calculated for different time differences Δt to see how much time can pass while the correlation of two delayed CIRs is kept above a certain level ρ. For the following, we choose $\rho = 0.5$.

In Figure 6 we can observe the Pearson correlation coefficient ρ as a function of the time lag Δt. We plot data for 7 passes of the vehicles and for $\Delta t \in [0, 2]$ s. The mean value of correlation is evaluated for the whole measurement region, i.e., $\mathrm{E}[\rho],\ \forall\ t \in [0, 4.6]$ s together with its variance depicted as the error bars. It is visible that the $\mathrm{E}[\rho] > 0.5$ for $\Delta t \in [0, 50]$ ms. In order to compare, in [23], for V2V channels at 5.6 GHz and with 240 MHz of bandwidth in a notably more rugged environment, the coherence times are in the range from 180 to 500 μs depending on the driving situation.

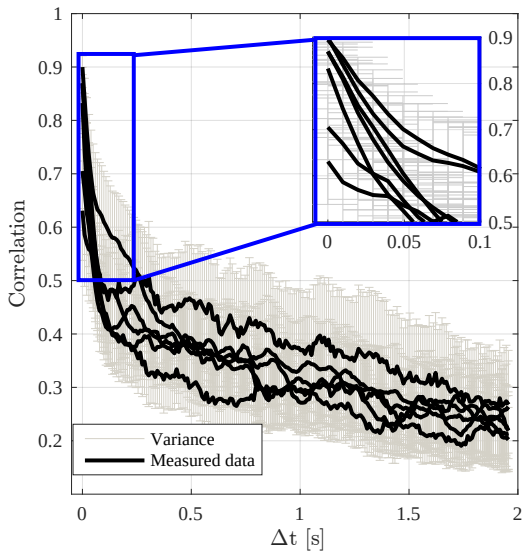

Fig. 6. Pearson correlation coefficient evaluation for several passes as a function of a correlation distance Δt.

In Figure 7 we show a dependency of $\mathrm{E}[\rho],\ \forall\ t \in [0, 4.6]$ s on the summed received power $\sum_\tau P(t,\tau)$ showing that the higher the total received power, the higher the correlations. The intuition is, that the lower the received power, the content of noise is proportionally higher, thus decreasing the correlation.

V. Conclusion

We have conducted broadband (with 8 GHz bandwidth) V2V mmwave channel measurements demonstrating the power-delay profiles of vehicles passing each other on a two-lane road. We evaluate the stationarity durations via a correlation between delayed channel impulse responses showing that in order to have mean correlations higher then 0.5, the time lag between measurements cannot be higher then 50 ms. Also, we show that the RMS delay spread increases with the received power. This poses an interesting problem, where usually the higher the signal-to-noise ratio (SNR), the lower the bit error rate (BER) of a hypothetical communication system without perfect channel state information (CSI). However, at the same time we show that the higher the received power (i.e. the SNR), the higher the RMS delay spread which usually also results in error floors and in the increase of the (uncoded) BER (as seen on page 242 in [21]). Therefore, the maximal transmit power possibly may not guarantee the lowest (uncoded) BER in the

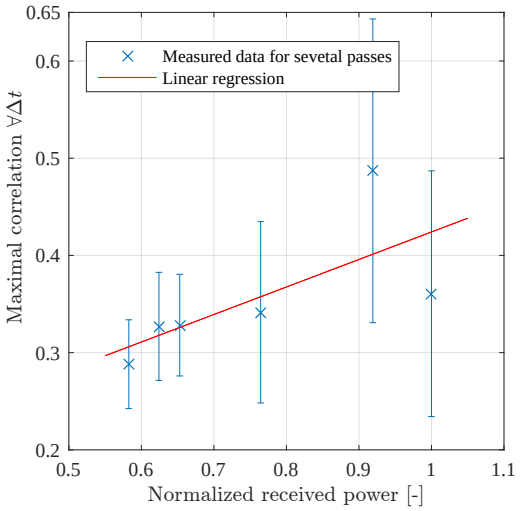

Fig. 7. Linear regression shows that the mean Pearson correlation coefficient (for all intended Δt) increases with the increase of the received power.

demonstrated scenario. In other words, for short distances, self-interference due to multipath components (MPCs) that fall outside the cyclic prefix or equalizer window might be the dominant effects of the characterized channels.

ACKNOWLEDGMENT

The research described in this abstract was financed by the Czech Science Foundation, Project No. 17-27068S, and by the National Sustainability Program under grant LO1401. For the research, the infrastructure of the SIX Center was used. The financial support by the Austrian Federal Ministry of Science, Research and Economy and the National Foundation for Research, Technology and Development is gratefully acknowledged. The work of AFM was supported by the California Transportation authority.

REFERENCES

[1] H. Meinel and A. Plattner, "Millimetre-wave propagation along railway lines," *IEE Proceedings F (Communications, Radar and Signal Processing)*, vol. 130, no. 7, pp. 688–694, 1983.

[2] T. S. Rappaport, S. Sun, R. Mayzus, H. Zhao, Y. Azar, K. Wang, G. N. Wong, J. K. Schulz, M. Samimi, and F. Gutierrez, "Millimeter wave mobile communications for 5G cellular: It will work!" *IEEE Access*, vol. 1, pp. 335–349, 2013.

[3] T. S. Rappaport, Y. Xing, G. R. MacCartney, A. F. Molisch, E. Mellios, and J. Zhang, "Overview of millimeter wave communications for fifth-generation (5G) wireless networks—with a focus on propagation models," *IEEE Transactions on Antennas and Propagation*, no. 12, pp. 6213–6230, 2017.

[4] H. Wang, X. Yin, X. Cai, H. Wang, Z. Yu, and J. Lee, "Fading characterization of 73 GHz millimeter-wave V2V channel based on real measurements," in *Communication Technologies for Vehicles*, J. Moreno García-Loygorri, A. Pérez-Yuste, C. Briso, M. Berbineau, A. Pirovano, and J. Mendizábal, Eds., Cham: Springer International Publishing, 2018, pp. 159–168.

[5] K. Akihito, S. Katsuyoshi, M. Fujise, and S. Kawakami, "Propagation characteristics of 60-GHz millimeter waves for ITS inter-vehicle communications," *IEICE Transactions on Communications*, vol. 84, no. 9, pp. 2530–2539, 2001.

[6] K. Sarabandi, E. S. Li, and A. Nashashibi, "Modeling and measurements of scattering from road surfaces at millimeter-wave frequencies," *IEEE Transactions on Antennas and Propagation*, vol. 45, no. 11, pp. 1679–1688, 1997.

[7] A. Yamamoto, K. Ogawa, T. Horimatsu, K. Sato, and M. Fujise, "Effect of road undulation on the propagation characteristics of inter-vehicle communications in the 60 GHz band," in *Proc. of IEEE/ACES International Conference on Wireless Communications and Applied Computational Electromagnetics*, 2005, pp. 841–844.

[8] J. Blumenstein, A. Prokes, J. Vychodil, M. Pospisil, and T. Mikulasek, "Time-varying K factor of the mm-wave vehicular channel: Velocity, vibrations and the road quality influence," in *IEEE 28th PIMRC*, 2017.

[9] J. Blumenstein, J. Vychodil, M. Pospisil, T. Mikulasek, and A. Prokes, "Effects of vehicle vibrations on mm-wave channel: Doppler spread and correlative channel sounding," in *IEEE 27th PIMRC*, 2016, pp. 1–5.

[10] Y. Wang, K. Venugopal, A. F. Molisch, and R. W. Heath, "Mmwave vehicle-to-infrastructure communication: Analysis of urban microcellular networks," *IEEE Transactions on Vehicular Technology*, vol. 67, no. 8, pp. 7086–7100, Aug. 2018.

[11] J. Blumenstein, A. Prokes, J. Vychodil, T. Mikulasek, J. Milos, E. Zöchmann, H. Groll, C. F. Mecklenbräuker, M. Hofer, D. Löschenbrand, L. Bernadó, T. Zemen, S. Sangodoyin, and A. Molisch, "Measured high-resolution power-delay profiles of nonstationary vehicular millimeter wave channels," in *IEEE 29th PIMRC*, Sep. 2018.

[12] E. Zöchmann, M. Hofer, M. Lerch, S. Pratschner, L. Bernadó, J. Blumenstein, S. Caban, S. Sangodoyin, H. Groll, T. Zemen, A. Prokeš, M. Rupp, A. F. Molisch, and C. F. Mecklenbräuker, "Position-specific statistics of 60 GHz vehicular channels during overtaking," *IEEE Access*, pp. 14 216–14 232, 2019.

[13] A. Prokes, J. Vychodil, T. Mikulasek, J. Blumenstein, E. Zöchmann, H. Groll, C. F. Mecklenbräuker, M. Hofer, D. Löschenbrand, L. Bernadó, T. Zemen, S. Sangodoyin, and A. Molisch, "Time-domain broadband 60 GHz channel sounder for vehicle-to-vehicle channel measurement," in *2018 IEEE Vehicular Networking Conference (VNC)*, Dec. 2018, pp. 1–7.

[14] T. Mikulasek, J. Lacik, and Z. Raida, "SIW slot antennas utilized for 60-GHz channel characterization," *Microwave and Optical Technol. Lett.*, vol. 57, no. 6, pp. 1365–1370, 2015.

[15] T. Mikulasek, J. Blumenstein, and A. Prokes, "Antennas utilized for intra-vehicle 3–11 GHz and 55–65 GHz channel measurement," in *2016 Progress in Electromagnetic Research Symposium (PIERS)*, Aug. 2016, pp. 4258–4262.

[16] F. Hlawatsch and G. Matz, *Wireless communications over rapidly time-varying channels*. Academic Press, 2011.

[17] M. Golay, "Complementary series," *IRE Transactions on Information Theory*, vol. 7, no. 2, pp. 82–87, Apr. 1961.

[18] R. J. Polge and E. M. Mitchell, "Impulse response determination by cross correlation," *IEEE Transactions on Aerospace and Electronic Systems*, vol. AES-6, no. 1, pp. 91–97, 1970.

[19] J. Vychodil, M. Pospisil, A. Prokes, and J. Blumenstein, "Millimetre wave band time domain channel sounder," *IET Communications*, vol. 13, no. 3, pp. 331–338, 2019.

[20] "LPRO rubidium oscillator for time and frequency reference. user's guide and integration guidelines," Datum Irvine, Tech. Rep., 2000.

[21] A. F. Molisch, *Wireless communications*. 2nd ed., Wiley - IEEE Press, 2011.

[22] J. Blumenstein, A. Prokes, A. Chandra, T. Mikulasek, R. Marsalek, T. Zemen, and C. Mecklenbrauker, "In-vehicle channel measurement, characterization, and spatial consistency comparison of 3-11 GHz and 55-65 GHz frequency bands," *IEEE Transactions on Vehicular Technology*, vol. 66, no. 5, pp. 3526–3537, May 2017.

[23] L. Bernadó, T. Zemen, F. Tufvesson, A. F. Molisch, and C. F. Mecklenbräuker, "Delay and doppler spreads of nonstationary vehicular channels for safety-relevant scenarios," *IEEE Trans. Veh. Technol.*, vol. 63, no. 1, pp. 82–93, 2014.